

**Zeolite-templated nanoporous carbon for high-performance supercapacitors**

Journal:	<i>Journal of Materials Chemistry A</i>
Manuscript ID	TA-ART-01-2018-000850.R1
Article Type:	Paper
Date Submitted by the Author:	18-Apr-2018
Complete List of Authors:	Lu, Hao; The University of Queensland, School of Chemical Engineering Kim, Kyoungsoo; Institute for Basic Science, d. Center for Nanomaterials and Chemical Reactions Kwon, Yonghyun; KAIST, Chemistry SUN, Xiaoming; The University of Queensland, School of Chemical Engineering Ryoo, Ryong; KAIST, ; IBS, Zhao, Xiu Song; The University of Queensland, School of Chemical Engineering



Zeolite-templated nanoporous carbon for high-performance supercapacitors

Hao Lu,^a Kyoungsoo Kim,^b Yonghyun Kwon,^{b,c} Xiaoming Sun,^a Ryong Ryoo,^{*a,b,c} and X. S. Zhao^{*a}

Received 00th January 20xx,
Accepted 00th January 20xx

DOI: 10.1039/x0xx00000x

www.rsc.org/

Hierarchical porous carbon prepared with calcium-containing nanocrystalline Beta zeolite as template and ethylene as carbon source at a relatively low carbonization temperature (600 °C) displayed excellent electrocapacitive properties. The presence of both micro/mesopores and surface oxygen-containing groups on the ordered porous structure, along with high specific surface area (2280 m²/g) and pore volume (1.95 cm³/g) coupled with good wettability towards the electrolyte enabled the carbon to perform well as supercapacitor electrode. This carbon electrode achieved a specific capacitance of 250 F/g at a current density of 1 A/g with 1 M H₂SO₄ as the aqueous electrolyte measured in a three-electrode system. A symmetric capacitor fabricated with the carbon as both electrodes exhibited a specific capacitance of 161 F/g at current density of 1 A/g, and an excellent cycling stability. After cycling 17000 times and shelved for another two months, the electrode exhibited a specific capacitance of 246 F/g at 1 A/g, 153 % of the initial capacitance, and still maintained an excellent cycle stability. Besides, an all-solid-state supercapacitor cell fabricated with this carbon as both electrodes and polyvinyl alcohol / H₂SO₄ gel as the electrolyte displayed an areal specific capacitance of 413 mF/cm² at a current density of 0.25 mA/cm².

Introduction

Supercapacitors (SCs) are energy storage devices with high power density and long life time.¹⁻³ Most currently available commercial SCs are fabricated with activated carbon (AC) as both electrodes, delivering a relatively low energy density.^{4,5} Alternative electrode materials other than AC have been actively searched.⁶⁻⁸

Hierarchically porous carbons (HPCs) with micropores, mesopores and/or macropores well-organised in three-dimension (3D) are ideal electrode materials for SCs.⁹ The micropores provide rich space for interacting with electrolyte ions. The mesopores and/or macropores function as ion reservoirs and low-resistant ion-transport tunnels, facilitating fast ion transport to and out of micropores.⁹⁻¹¹

The zeolite template method has been widely used to prepare HPCs.¹²⁻¹⁷ In this method, it has been challenging to selectively deposit carbon in zeolite micropores for preparing highly ordered HPCs^{18,19} because a carbon precursor tends to deposit on the external surface of the template.²⁰ Therefore, the structure of currently available HPCs prepared using the template method contains mainly meso/macropores rather than micro/mesopores, which are more desirable in the development of carbon electrode materials for electrical double layer capacitors (EDLCs).^{21,22}

Recently, we reported the use of nano-sized Beta zeolite as the template to prepare HPCs with a micropore-mesopore hierarchy.²³ Subsequently, we demonstrated that microporous carbons with graphene-like pore walls can be readily prepared by using lanthanum-zeolite template.²⁴ In this work, we employed calcium-containing nano-sized Beta zeolite as template and ethylene as the carbon precursor to prepare HPCs. In comparison with other samples templated from micro-sized zeolites Y and Beta, the nano-sized zeolite Beta template carbon exhibited the best electrocapacitive performance due to the presence of mesopores, which facilitate the ion and electron transport for both EDLC and pseudocapacitance.

Experimental section

Preparation of zeolite-templated carbon

Both zeolites Y (denoted as YZ) and Beta (denoted as BZ) were purchased from Tosoh Corp. Nano-sized Beta zeolite (denoted as NBZ) was synthesized as described elsewhere.²⁵ Ethylene was used as the carbon precursor. A zeolite template (YZ or BZ or NBZ) was placed in a vertical fused quartz reactor equipped with a fritted disk (see Fig. S1). The template was heated to 600 °C under dry N₂ gas flow. A mixture of ethylene gas, steam and nitrogen was then passed through the zeolite bed. After the carbon deposition was completed, the gas flow was switched to dry N₂ and the temperature was increased to 850 °C and maintained at this temperature for 2 h. The template was washed away with a HF/HCl solution. Samples were washed with deionised water to remove residual chemicals and dried at 150 °C for 48 h. Three carbon replica of YZ, BZ and NBZ were

^a School of Chemical Engineering, The University of Queensland, St Lucia, Brisbane, QLD 4072, Australia. *E-mail: george.zhao@uq.edu.au (X. S. Zhao)

^b Center for Nanomaterials and Chemical Reactions, Institute for Basic Science (IBS), Daejeon 34141, Republic of Korea.

^c Department of Chemistry, KAIST, Daejeon 34141, Republic of Korea. *E-mail: rryoo@kaist.ac.kr (R. Ryoo)

Electronic Supplementary Information (ESI) available. See DOI: 10.1039/x0xx00000x

obtained and the samples are denoted as YZC, BZC and NBZC, respectively.

Characterization

X-Ray diffraction (XRD) patterns were recorded on a Rigaku Multiplex instrument using Cu K α radiation (30 kV, 40mA). Raman spectra were collected using a Raman spectrometer (Renishaw) with a 514 nm laser. Nitrogen adsorption/desorption isotherms were measured using a Micromeritics Tristar II volumetric adsorption analyzer at liquid N₂ temperature after all samples were degassed at 300 °C for 4 h. Ar sorption isotherms were measured using a Micromeritics ASAP 2020 volumetric adsorption analyzer at liquid Ar temperature. The specific surface area (SSA) of the samples were calculated using the Brunauer–Emmett–Teller (BET) method using data points within a relative pressure range of 0.05–0.2. The total pore volume was estimated at P/P₀ = 0.95. The micropore volume was determined by t-plot method. The mesopore size distributions were determined through Nitrogen adsorption isotherms using Barrett–Joyner–Halenda (BJH) model. The micropore size distributions were determined through Ar adsorption isotherms using quantized liquid density-functional theory (DFT) model, assuming a slit-shaped pore geometry. Scanning electron microscopy (SEM) images were collected on a Verios 460 (FEI) at a landing voltage of 1 kV in deceleration mode (stage bias voltage: 5 kV). Transmission electron microscopy (TEM) images were collected with a Titan E-TEM G2 (FEI) at an acceleration voltage of 300 kV, on a holey carbon grid (300 mesh) after supporting with ethanol dispersion. X-ray photoelectron spectroscopy (XPS) spectra were acquired by a Thermo Fisher Scientific Sigma probe with a monochromated Al K α X-ray source.

Electrochemical measurement

The working electrodes were prepared by mixing 75 wt% active materials, 20 wt% carbon black as a conductive additive and 5 wt% polytetrafluoro ethylene (PTFE) binder. Then the mixture was pressed onto a stainless-steel mesh and dried at 60 °C for 48 h. A Whatman filter paper (GF/D) was used as the separator. The mass loading of active materials on each current collector was ~2 mg/cm². Cyclic voltammetry (CV), galvanostatic charge–discharge (GCD) and electrochemical impedance spectroscopy (EIS) measurements were all conducted at room temperature using an Autolab PGSTAT 3020 N.

Electrochemical measurement in aqueous electrolyte system

The electrolyte was 1 M H₂SO₄ aqueous solution. For the three-electrode system, Hg/HgO and Ag/AgCl were used as the counter and reference electrode, respectively. For the two-electrode system, a symmetric SC using the same mass loading (~2 mg) on both electrodes was assembled. CV scans were obtained at various scan rates in the range of 5 – 200 mV/s. GCD cycling for the three-electrode and two-electrode systems was performed at current

densities ranging from 0.2 to 20 A/g and 0.1 to 10 A/g, respectively. The EIS measurement was carried out at an open circuit potential with an amplitude of 5 mV in the frequency range of 10 mHz – 100 kHz.

Electrochemical measurement of all-solid-state SCs

The polyvinyl alcohol / H₂SO₄ gel electrolyte was prepared as follows:²⁶ 3 g polyvinyl alcohol (PVA) was added into 30 ml 1M H₂SO₄ aqueous solution and stirred for 1 h. Subsequently, the mixture was heated to 80 °C under vigorous stirring until the whole solution became clear. Then working electrodes and the separator were soaked with the PVA/H₂SO₄ gel electrolyte and solidified at room temperature for 24 h before they were assembled together. The working electrode had an area mass loading of ~2 mg/cm² and the active materials had an area of ~1 cm². CV scans of the symmetric all-solid-state cell were conducted at various scan rates in the range of 5 – 100 mV/s. The GCD tests were performed at current densities ranging from 0.25 to 20 mA/cm². The EIS measurement was also conducted in the frequency range of 10 mHz – 100 kHz at an amplitude of 5 mV referring to open circuit potential.

The mass based specific capacitance C_s (in F/g) measured on a three-electrode system was calculated from the galvanostatic discharge process using the following equation:

$$C_s = I\Delta t / mV \quad (1)$$

The C_s value derived from the GCD data measured on a two-electrode system was calculated from the following equation:

$$C_s = 4I\Delta t / 2mV \quad (2)$$

The areal capacitance C_a (in mF/cm²) measured on a two-electrode system was calculated from the following equation:

$$C_a = 4I\Delta t / 2SV \quad (3)$$

where, I is the instantaneous current, Δt is the discharge time, m is the mass of the active materials on a single electrode, S is the superficial area of the active materials on a single electrode and V is the potential window.

The volumetric energy density, E_v (in mWh/cm³), and volumetric power density, P_v (in mW/cm³), of an all-solid-state SC were obtained through the following equations:

$$E_v = E / V_{device} \quad (4)$$

$$P_v = 3.6E_v / V_{device} \quad (5)$$

Where V_{device} is the volume of the whole device.

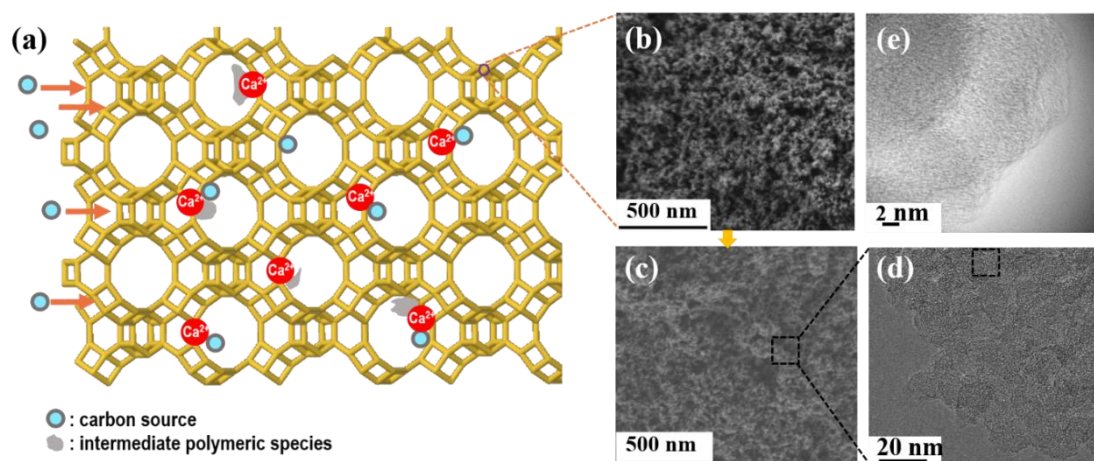


Fig. 1. (a) A schematic diagram showing the preparation of carbon deposition in calcium-containing zeolite templates, SEM images of (b) template NBZ and (c) resultant carbon replica NBZC, (d) TEM, (e) HRTEM image of NBZC.

Results and discussion

Fig. 1a schematically shows the preparation process of carbon samples using calcium-containing zeolites as the templates. The SEM images (shown in Fig. 1, and Fig. S2) and TEM images (shown in Fig. 1 and Fig. S3) show that the three samples are good replica of their separate template. More details about their preparation process and characterisations can be seen in the Supporting Information. In this paper we will mainly focus on the measurement and interpretation of their electrocapacitive performance.

Firstly, the electrochemical performance was investigated by using CV, GCD and EIS techniques in a three-electrode system with 1 M H_2SO_4 as the aqueous electrolyte at a potential window between -0.3 and 0.7 V vs. Ag/AgCl. Fig. 2a shows the CV profiles of samples measured at a scan rate of 5 mV/s. All of them exhibit a quasi-rectangular shape with redox peaks due to the pseudocapacitive faradic reactions of oxygen-containing functional groups, especially NBZC, indicating a better utilisation of oxygen groups on account of a hierarchically porous structure. Besides, the NBZC electrode showed an increased current density compared with other two electrodes, suggesting a better capacitive performance.²⁷ The rate capability of them is shown in Fig. 2b. The electrode NBZC showed a much better rate capability than YZC and BZC, which is further supported by EIS results in Fig. 2c. The Nyquist plots show that the electrode NBZC had a much smaller charge resistance than the other two electrodes.

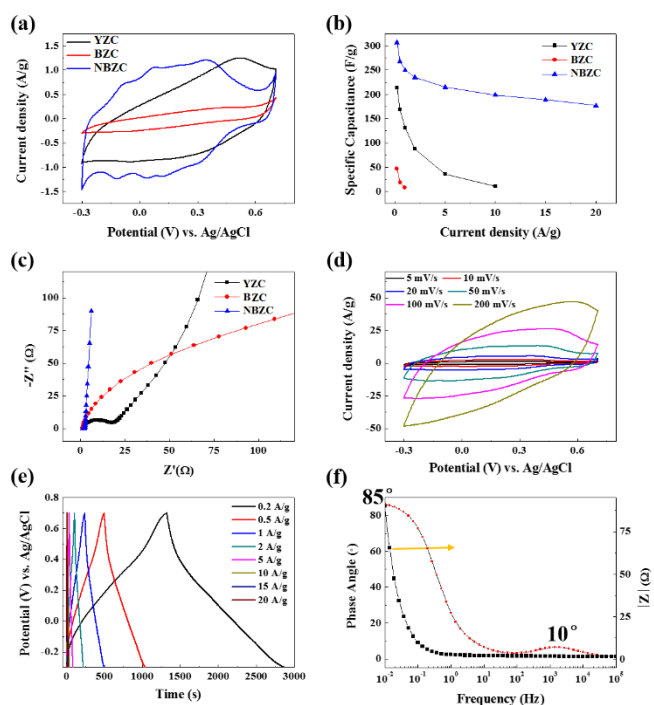


Fig. 2. Electrocapacitive properties of different electrode materials measured using a three-electrode system with 1 M H_2SO_4 as aqueous electrolyte: (a) CV curves at a scan rate of 5 mV/s, (b) rate capability, and (c) EIS curves. (d) CV curves at scan rates ranging from 5 mV/s to 200 mV/s, (e) GCD curves at current densities ranging from 0.2 A/g to 20 A/g, and (f) Bode plots of electrode NBZC.

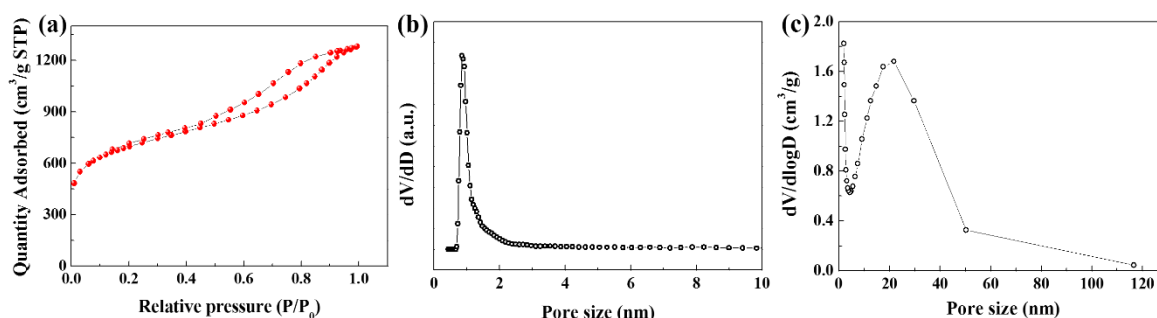


Fig. 3. N₂ adsorption/desorption isotherms (a) and pore size distribution curves calculated using the DFT model (b) and BJH model (c).

Table 1. Textual properties of the samples.

Sample	S_{BET} (m ² /g)	V_{total} (cm ³ /g)	V_{micro} (cm ³ /g)	V_{micro}/V_{total} (%)
YZC	2220	1.12	0.89	79.5
BZC	2770	1.39	0.91	65.5
NBZC	2280	1.95	0.65	33.3

S_{BET} : the specific surface area from BET. V_{total} (cm³/g): total pore volume estimated at $P/P_0 = 0.95$. V_{micro} : volume of micropores calculated by the t-plot method.

As NBZC showed the best electrocapacitive performance among these three samples, subsequent investigations were focused on this sample. Figs. 2d and 2e show the CV and GCD curves of NBZC, respectively. It can be seen all CV curves exhibit a quasi-rectangular shape while all GCD curves display a quasi-triangle shape, indicating both electric double layer and pseudocapacitive contributions. At a faster scan rate, the CV curve was slightly distorted, implying that some pseudocapacitive species could not participate in the faradic redox reactions at very fast scan rates.²⁷ However, the electrode still showed a good rate capability as seen from the data in Fig. 2b and Table S1. The specific capacitance was 307 F/g at a current density of 0.2 A/g, and it remained 177 F/g at current density of 20 A/g.

Fig. 3a shows the N₂ adsorption/desorption isotherms of NBZC. The presence of a hysteresis loop indicates the existence of mesopores. The textual properties of the three samples are compared in Table 1. All three samples have a SSA of higher than 2200 m²/g. In comparison with other two samples, NBZC possesses the highest pore volume (1.95 cm³/g) and lowest ratio of micropore volume over total pore volume, indicating a significant contribution of mesopores to the total pore volume. Figs. 3b and 3c show the well-controlled pore size distribution of NBZC calculated from the DFT model and BJH model, respectively. It exhibits prominent micropore and mesopore peaks centred at 1 nm and 20 nm, respectively. The micropores provide sufficient active sites for EDLC and mesopores enable active ions in micropores to have nanometre transport distances.^{9, 28-31} In comparison, as shown in Fig. S6, YZC and BZC only exhibit a

prominent micropore peak centred at 1 nm, which leads to a larger charge resistance and electrolyte diffusion resistance thus an ordinary rate capability. Moreover, compared with chemical activation, the zeolite template method can afford a more ordered straight hierarchical porous structure. That enables the carbon electrode NBZC to have low-resistant, as shown by the Nyquist plots in Figs. 2c and S5, ion-transport paths, which is beneficial for both the rate capability and power density.^{2, 32, 33}

Furthermore, the good wettability of NBZC benefitting from a certain degree of graphitization further enhances the ion transfer efficiency.²⁹ The HRTEM image in Fig. 2e shows a certain degree of graphitization of NBZC which is consistent with the Raman spectroscopy results in Fig. S7, showing a much higher intensity of G-band than D-band. This is beneficial for the surface wettability as well as the electronic conductivity of NBZC as the electrode.³⁴

Figs. 4a and S8a shows the XPS survey spectra of the three samples. The quantitative analysis showed that they contained a similar content of oxygen – 9.9 at%, 10.6 at%, 9.2 at%, respectively. But as can be seen from the CV profiles in Fig. 2a, the oxygen functional groups of NBZC were better utilised. That maybe because of the well-organised hierarchically porous structure, which enables the electrolyte ions to have more sufficient interact with the oxygen groups evenly spreading on the carbon NBZC, supported by Fig. S9. In summary, the excellent performance of NBZC is on account of

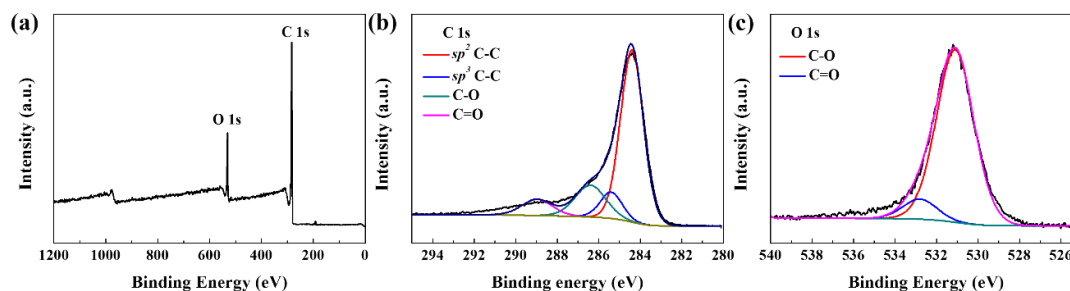


Fig. 4. XPS survey spectra of NBZC (a), and the deconvoluted C 1s (b), O 1s spectra (c).

the ordered straight hierarchical porous structure originating from the zeolite template method and pseudocapacitance contribution from the evenly spread oxygen-containing surface groups on it, as well as the good wettability towards the electrolyte.

The electrochemical performance of electrode NBZC was further assessed in a symmetric cell with 1 M H₂SO₄ as the aqueous electrolyte. As shown in Fig. 5a, the CV curves exhibit a quasi-rectangular shape characteristic of a combined contribution of EDLC and pseudocapacitance.³⁴ And the CV curve only shows limited distortion at a high scan rate of 200 mV/s, indicating a good rate capability of the cell. Fig. 5b shows the GCD curves of this cell at different current densities ranging from 0.1 A/g to 10 A/g. All these curves exhibit a quasi-linear shape demonstrating both EDLC and pseudocapacitance, in consistency with the CV tests. The cell electrode exhibited a specific capacitance of 170 F/g at 0.1 A/g. Fig. 5c shows the rate capability of the symmetric cell. The capacitance at a high current density of 10 A/g remained approximately 60 % of the value at 0.1 A/g. Comparisons of the preparation, structural and electrocapacitive properties of NBZC with other HPCs reported recently are shown in Table. S2.

Fig. 5d shows the Nyquist plot of the cell. It consists of a semicircle in the high-frequency region and an almost vertical line in the low-frequency region. The almost vertical line in the low-frequency region reveals that EDLC is the dominant capacitance contribution of the cell, consistent with both CV and GCD results. The equivalent circuit shown in Fig.S10 was used to simulate the impedance response of the cell.³⁵⁻³⁸ R_s stands for the summarization of contact resistance, electrolyte resistance and the bulk resistance of the electrode. R_{ct} is the resistance caused by charge transfer for both EDLC and pseudocapacitance.³⁹ The constant phase element Q_{dl} represents a part of the capacitance at the high and medium frequency. Z_w represents the electrolyte diffusion resistance, i.e., Warburg impedance.³⁷ C_m is the main capacitance at low frequency.

R_L is the leakage resistance which is relatively high and usually ignored in the circuit. Figs. 5d and 5e show that excellent fitting results were obtained for both the Nyquist plot and Bode plots. The Nyquist plot shows that the cell had low-value R_s and R_{ct} of 1.43 Ω

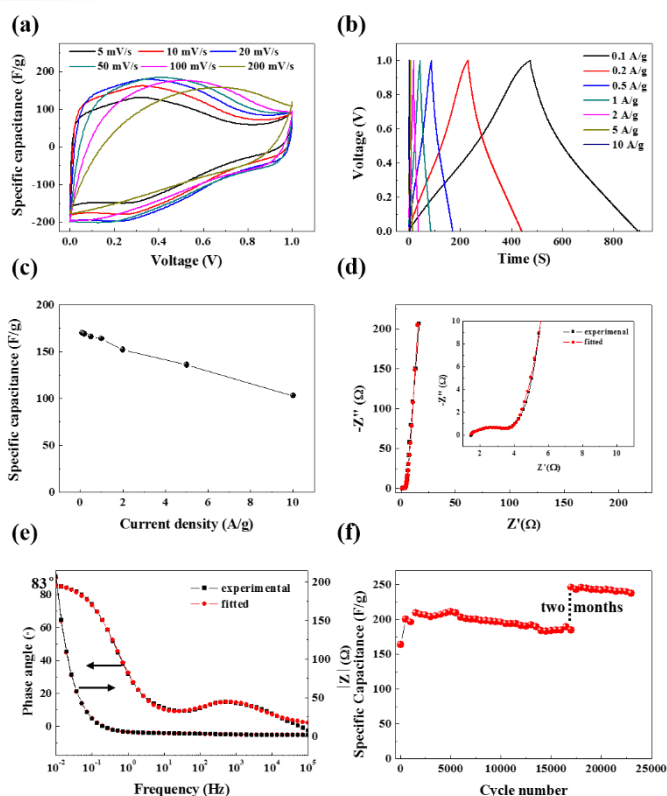


Fig. 5. Electrocapacitive performance of electrode NBZC in a symmetric cell with 1 M H₂SO₄ as aqueous electrolyte: (a) CV curves at scan rates from 5 mV/s to 200 mV/s, (b) GCD curves at current densities from 0.1 A/g to 10 A/g, (c) rate capability, (d) Nyquist plot, (e) Bode plots, and (f) cycling stability at 1 A/g.

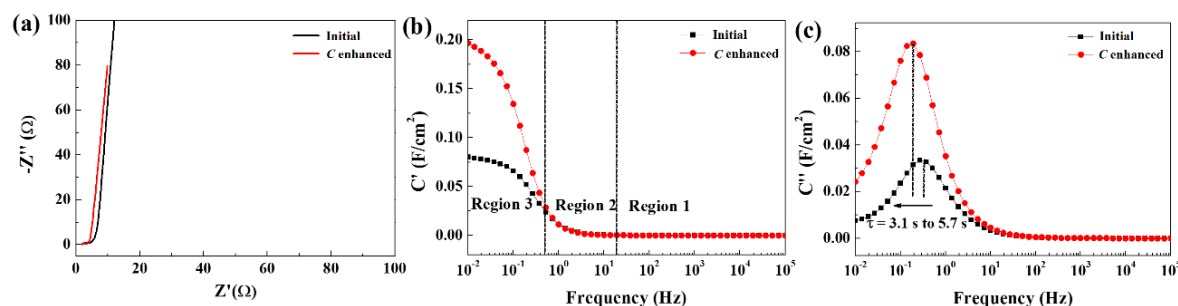


Fig. 6. Nyquist plots (a), real part capacitance (b) and imaginary capacitance (c) vs. frequency for electrode NBZC in a symmetric cell with 1 M H_2SO_4 as the electrolyte.

and 2.38Ω respectively. The relatively low equivalent series resistance, the sum of R_s and R_{ct} , i.e., 3.81Ω , and short Warburg region benefiting from the ordered hierarchical porous structure and certain degree of graphitization, enable the cell to show a good rate capability.^{39, 40} The Bode phase angle plot (Fig. 5e) exhibit two maximum values and a phase angle of 83° at low frequency region, which further proves the coexistence of EDLC and pseudocapacitance.⁴¹

Long cycle life is one of the critical impactors for the application of SCs. As shown in Fig. 5f, the specific capacitance of this SC electrode showed an apparent increase after certain cycles. The capacitance enhancement was further studied through the EIS technique as shown in Fig. 6 and Fig. S11. The electrode retained approximately 120 % of the initial capacitance after 17000 cycles at the current density of 1 A/g. The slight capacitance value fluctuation may be associated with the minor temperature variation during the long-term cycling test to some extent.⁴²⁻⁴⁴

Fig. 6a shows that the cell exhibited similar R_s but much lower R_{ct} and Z_w after certain cycles the capacitance enhanced. In consistence with Fig. 6a, Fig. S11a also shows that the real part resistance, containing R_s , R_{ct} and Z_w , was much lower. The lower resistance facilitates electron transport thus enables the cell to exhibit a better electrochemical performance.⁴⁵ Fig. 6b presents the real part specific capacitance (C') vs. frequency. The C' showed almost no change in region 1 and region 2. But in region 3, the value of C' significantly enhanced. This indicates that the capacitance improvement is due to a more efficient utilisation of micropores, which means a higher electrochemically accessible surface area for the cell. The longer soaking time and certain number of GCD tests enable more micropores, especially the inner-region micropores, to be accessed by sufficient electrolyte, thus providing more electrochemical active sites.⁴⁶ Fig. 6c presents the imaginary specific capacitance (C'') vs. frequency. The C'' showed a maximum value at a frequency of f_0 , defining a time constant of $\tau_0 = 1 / f_0$. It can be seen that the τ_0 increased from 3.1 s to 5.7 s. Although the more efficient utilisation of inner-region micropores enhanced the capacitance value, it also increased the relaxation time due to a relatively lengthening diffusion pathways for ion transport.⁴⁷ The Fig. S11b further confirms the increase of τ_0 . Therefore, the cell showed a higher specific capacitance and energy density but meanwhile a reduced power density to some extent.^{38, 48}

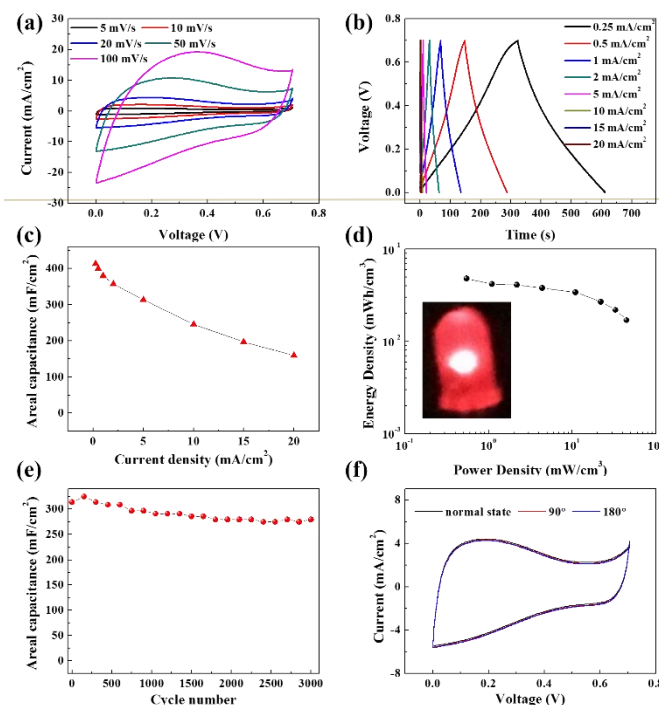


Fig. 7. Electrocapacitive performance of NBZC in an all-solid-state symmetric cell with PVA/ H_2SO_4 gel as the electrolyte: (a) CV curves at different scan rates, (b) GCD curves at different current densities, (c) rate capability, and (d) a Ragone plot of volumetric energy density versus volumetric power density (the inset shows a 2.3 V LED powered by 3 SC cells connected in series), (e) cycling stability at 5 mA/cm^2 , (f) CV curves at 20 mV/s with different bending angles.

More interestingly, as shown in Fig. 5f, the specific capacitance at the current density of 1 A/g further increased to 246 F/g, 153 % of the initial value, shelved another 2 months after the 17000 cycling tests, and it still maintained an excellent cycle stability. The possible reasons for the superior cycle life of this electrode are: (a) the ordered straight hierarchical porous structure, it enables an excellent charge transfer and ion transport network²⁸ and facilitates an efficient use of pseudocapacitance from oxygenated functionalities;^{2, 14, 42, 49} (b) certain graphitization degree, which is also beneficial for the electron and ion transfer;⁵⁰ and (c) a relatively higher H^+ concentration after a long time, which might also contribute to the further capacitance increase. In our future work, further research on capacitance enhancement after long-term tests will be conducted.

Fig. 7 shows the electrochemical performance of electrode NBZC in an all-solid-state cell with PVA/H₂SO₄ gel as the electrolyte. A high areal specific capacitance of 413 mF/cm² was obtained at a current density of 0.25 mA/cm². And it remained at 380 mF/cm², 246 mF/cm², 160 mF/cm² at current densities of 1 mA/cm², 10 mA/cm², 20 mA/cm² respectively. Relatively high volumetric energy density and power density based on the whole device were obtained and three such capacitors connected in series can light a commercial red light-emitting diode (LED, 2.3 V) as shown in Fig. 7d. The all-solid-state cell also exhibited a good cycling stability as shown in Fig. 7e. The areal capacitance value remained around 89 % after 3000 cycles at a current density of 5 mA/cm². Fig. 7f shows the CV curves of the cell at a scan rate of 20 mV/s. The curves showed no visible change at different bending state, demonstrating its potential as a flexible device.

Conclusions

With ethylene as the carbon source and calcium-containing nano Beta zeolite as the template, 3D micro/mesoporous carbons of high specific surface area were prepared at a relatively low carbonization temperature, 600 °C. The Ca²⁺ localized in micropores of zeolite can strongly interact with ethylene, leading to selective deposition of carbon in pores instead of on the external surface of the template. A comparative study of carbons prepared with different zeolite templates indicated that the sample prepared using nano Beta zeolite displayed the best electrocapacitive performance because of the well-controlled hierarchical porous structure and pseudocapacitance contribution from oxygen-containing surface groups evenly spread on it, as well as the good wettability towards the electrolyte. This carbon exhibited an excellent stability against cycling. The carbon electrode was cycled 17000 times in a symmetric cell with 120% capacity remained. The EIS data indicates that the capacitance improvement is due to a more efficient use of micropores. The long soaking time and certain number cycling tests enabled more micropores to be accessed by sufficient electrolyte, thus providing more electrochemically active sites. Furthermore, two-month shelving time after 17000 cycling tests, this electrode was cycled again at 1 A/g. The capacitance reached 246 F/g and it still maintained an excellent cycling stability. The superior cycle life of this carbon is on account of the ordered straight micro-mesopore hierarchy, certain graphitization degree and the relatively higher H⁺ concentration after a long soaking time. More research on the capacitance further enhancement after the two-month shelving time is needed in our future work. This carbon also exhibited good performance in an all-solid-state SC with PVA/H₂SO₄ gel as the electrolyte. A high areal specific capacitance of 413 mF/cm² was obtained at a current density of 0.25 mA/cm². Moreover, the experimental procedure for preparing zeolite-templated carbon can be scaled up as shown in Fig. S1. With 40 g of zeolite template, about 13 g carbon can be obtained.

Conflicts of interest

There are no conflicts to declare.

Acknowledgements

The acknowledgements come at the end of an article after the conclusions and before the notes and references. The Australian Research Council is acknowledged for supporting this research work (FL170100101). The UQ Vice-Chancellor's Research and Teaching Fellowship Program (2015000144) is also acknowledged. R. R., K. K, and Y. K. acknowledge support from the Institute for Basic Science under grant number IBS-R004. H. L wishes to thank the UQ-CSC program for providing a scholarship.

Notes and references

1. P. Simon and Y. Gogotsi, *Nature materials*, 2008, **7**, 845-854.
2. L. L. Zhang and X. Zhao, *Chemical Society Reviews*, 2009, **38**, 2520-2531.
3. P. Simon, Y. Gogotsi and B. Dunn, *Science Magazine*, 2014, **343**, pp. 1210-1211.
4. T. Lin, I.-W. Chen, F. Liu, C. Yang, H. Bi, F. Xu and F. Huang, *Science*, 2015, **350**, 1508-1513.
5. L. L. Zhang, Y. Gu and X. Zhao, *Journal of Materials Chemistry A*, 2013, **1**, 9395-9408.
6. R. R. Salunkhe, Y. H. Lee, K. H. Chang, J. M. Li, P. Simon, J. Tang, N. L. Torad, C. C. Hu and Y. Yamauchi, *Chemistry-A European Journal*, 2014, **20**, 13838-13852.
7. R. R. Salunkhe, J. Tang, N. Kobayashi, J. Kim, Y. Ide, S. Tominaka, J. H. Kim and Y. Yamauchi, *Chemical Science*, 2016, **7**, 5704-5713.
8. J. Tang and Y. Yamauchi, *Nature chemistry*, 2016, **8**, 638.
9. D. W. Wang, F. Li, M. Liu, G. Q. Lu and H. M. Cheng, *Angewandte Chemie*, 2008, **120**, 379-382.
10. X. Zheng, J. Luo, W. Lv, D. W. Wang and Q. H. Yang, *Adv Mater*, 2015, **27**, 5388-5395.
11. X. Fan, C. Yu, J. Yang, Z. Ling, C. Hu, M. Zhang and J. Qiu, *Advanced Energy Materials*, 2015, **5**, 14011761.
12. T. Kyotani, T. Nagai, S. Inoue and A. Tomita, *Chemistry of materials*, 1997, **9**, 609-615.
13. C. J. Meyers, S. D. Shah, S. C. Patel, R. M. Sneeringer, C. A. Bessel, N. R. Dollahon, R. A. Leising and E. S. Takeuchi, *The Journal of Physical Chemistry B*, 2001, **105**, 2143-2152.
14. X. S. Zhao, F. Su, Q. Yan, W. Guo, X. Y. Bao, L. Lv and Z. Zhou, *Journal of Materials Chemistry*, 2006, **16**, 637-648.
15. W. Xia, B. Qiu, D. Xia and R. Zou, *Scientific reports*, 2013, **3**.
16. X. Wen, D. Zhang, T. Yan, J. Zhang and L. Shi, *Journal of Materials Chemistry A*, 2013, **1**, 12334-12344.
17. X. Y. Chen, C. Chen, Z. J. Zhang and D. H. Xie, *Journal of Materials Chemistry A*, 2013, **1**, 10903-10911.
18. Z. Li, D. Wu, Y. Liang, R. Fu and K. Matyjaszewski, *J Am Chem Soc*, 2014, **136**, 4805-4808.
19. H. Nishihara and T. Kyotani, *Adv Mater*, 2012, **24**, 4473-4498.
20. H. Xu, Q. Gao, H. Guo and H. Wang, *Microporous and Mesoporous Materials*, 2010, **133**, 106-114.
21. J. Chmiola, G. Yushin, Y. Gogotsi, C. Portet, P. Simon and P.-L. Taberna, *Science*, 2006, **313**, 1760-1763.
22. D. Hulicova-Jurcakova, A. M. Puziy, O. I. Poddubnaya, F. Suárez-García, J. M. Tascón and G. Q. Lu, *J Am Chem Soc*, 2009, **131**, 5026-5027.
23. K. Kim, M. Choi and R. Ryoo, *Carbon*, 2013, **60**, 175-185.

24. K. Kim, T. Lee, Y. Kwon, Y. Seo, J. Song, J. K. Park, H. Lee, J. Y. Park, H. Ihee and S. J. Cho, *Nature*, 2016, **535**, 131-147.
25. M. Choi, K. Na and R. Ryo, *Chemical Communications*, 2009, 2845-2847.
26. X. Lu, M. Yu, G. Wang, Y. Tong and Y. Li, *Energy & Environmental Science*, 2014, **7**, 2160-2181.
27. Z. Lei, L. Lu and X. S. Zhao, *Energy & Environmental Science*, 2012, **5**, 6391-6399.
28. H. Lu and X. Zhao, *Sustainable Energy & Fuels*, 2017, **1**, 1265-1281.
29. L. Qie, W. Chen, H. Xu, X. Xiong, Y. Jiang, F. Zou, X. Hu, Y. Xin, Z. Zhang and Y. Huang, *Energy & Environmental Science*, 2013, **6**, 2497-2504.
30. M. Biswal, A. Banerjee, M. Deo and S. Ogale, *Energy & Environmental Science*, 2013, **6**, 1249-1259.
31. G. Zhang and X. W. D. Lou, *Adv Mater*, 2013, **25**, 976-979.
32. H. Jiang, J. Ma and C. Li, *Adv Mater*, 2012, **24**, 4197-4202.
33. H. J. Liu, J. Wang, C. X. Wang and Y. Y. Xia, *Advanced Energy Materials*, 2011, **1**, 1101-1108.
34. H. Lu, X. Sun, R. R. Gaddam, N. A. Kumar and X. S. Zhao, *Journal of Power Sources*, 2017, **360**, 634-641.
35. C. Masarapu, H. F. Zeng, K. H. Hung and B. Wei, *ACS nano*, 2009, **3**, 2199-2206.
36. W. Wang, S. Guo, I. Lee, K. Ahmed, J. Zhong, Z. Favors, F. Zaera, M. Ozkan and C. S. Ozkan, *Scientific reports*, 2014, **4**.
37. S. K. Meher and G. R. Rao, *The Journal of Physical Chemistry C*, 2011, **115**, 15646-15654.
38. P. Taberna, P. Simon and J.-F. Fauvarque, *Journal of The Electrochemical Society*, 2003, **150**, A292-A300.
39. J. Zhang and X. Zhao, *ChemSusChem*, 2012, **5**, 818-841.
40. A. Di Fabio, A. Giorgi, M. Mastragostino and F. Soavi, *Journal of the Electrochemical Society*, 2001, **148**, A845-A850.
41. B. E. Conway, *Journal of the Electrochemical Society*, 1991, **138**, 1539-1548.
42. Y. Wang, W. Lai, N. Wang, Z. Jiang, X. Wang, P. Zou, Z. Lin, H. J. Fan, F. Kang and C.-P. Wong, *Energy & Environmental Science*, 2017, **10**, 941-949.
43. F. Rafik, H. Gualous, R. Gallay, A. Crausaz and A. Berthon, *Journal of power sources*, 2007, **165**, 928-934.
44. S. Dutta, A. Bhaumik and K. C.-W. Wu, *Energy & Environmental Science*, 2014, **7**, 3574-3592.
45. Y. Deng, C. Liu, T. Yu, F. Liu, F. Zhang, Y. Wan, L. Zhang, C. Wang, B. Tu and P. A. Webley, *Chemistry of materials*, 2007, **19**, 3271-3277.
46. L.-F. Chen, Y. Lu, L. Yu and X. W. D. Lou, *Energy & Environmental Science*, 2017.
47. J. Chmiola, G. Yushin, R. Dash and Y. Gogotsi, *Journal of Power Sources*, 2006, **158**, 765-772.
48. C. Portet, P. L. Taberna, P. Simon, E. Flahaut and C. Laberty-Robert, *Electrochimica Acta*, 2005, **50**, 4174-4181.
49. C. O. Ania, V. Khomenko, E. Raymundo - Piñero, J. B. Parra and F. Beguin, *Advanced Functional Materials*, 2007, **17**, 1828-1836.
50. L. Sun, C. Tian, M. Li, X. Meng, L. Wang, R. Wang, J. Yin and H. Fu, *Journal of Materials Chemistry A*, 2013, **1**, 6462-6470.